Eur. J. Mineral., 34, 523–538, 2022
https://doi.org/10.5194/ejm-34-523-2022

European Journal of Mineralogy
Open Access

TotBlocks: exploring the relationships between modular rock-forming minerals with 3D-printed interlocking brick modules

Derek D. V. Leung[1,2] **and Paige E. dePolo**[1]

[1]School of GeoSciences, The University of Edinburgh, Edinburgh, United Kingdom
[2]Harquail School of Earth Sciences, Laurentian University, Sudbury, Ontario, Canada

Correspondence: Derek D. V. Leung (dleung@laurentian.ca)

Received: 9 August 2022 – Revised: 28 September 2022 – Accepted: 29 September 2022 – Published: 1 November 2022

Abstract. Many rock-forming chain and sheet silicate minerals, i.e., pyroxenes, amphiboles, micas, and clay minerals, are built from shared chemical building blocks known as T-O-T modules. Each module consists of two opposing chains of vertex-sharing silica tetrahedra (T), which vertically sandwich a ribbon of edge-sharing metal–oxygen octahedra (O) in a T-O-T configuration. These minerals are both abundant and diverse in the lithosphere because T-O-T modules are chemically versatile (incorporating common crustal elements, e.g., O, Si, Al, Fe, and Mg) and structurally versatile (varying as a function of module width and linkage type) over a wide range of chemical and physical conditions. Therefore, these minerals lie at the center of understanding geological processes. However, their diversity leads to the minerals developing complex, 3D crystal structures, which are challenging to communicate. Ball-and-stick models and computer visualization software are the current methods for communicating the crystal structures of minerals, but both methods have limitations in communicating the relationships between these complex crystal structures. Here, we investigate the applications of 3D printing in communicating modular mineralogy and crystal structures. The open-source TotBlocks project consists of 3D-printed, T-O-T interlocking bricks, based on ideal polyhedral representations of T and O modules, which are linked by hexagonal pegs and slots. Using TotBlocks, we explore the relationships between modular minerals within the biopyribole (biotite–pyroxene–amphibole) and palysepiole (palygorskite–sepiolite) series. The bricks can also be deconstructed into T and O layer modules to build other mineral structures such as the brucite, kaolinite–serpentine, and chlorite groups. Then, we use the T-O-T modules within these minerals to visually investigate trends in their properties, e.g., habit, cleavage angles, and symmetry/polytypism. In conclusion, the TotBlocks project provides an accessible, interactive, and versatile way to communicate the crystal structures of common rock-forming minerals.

Graphical abstract

The graphical abstract highlights how TotBlocks links modular mineralogy to mineral properties: (a) the pyroxene structure, illustrating cleavages between T-O-T rod modules; (b) its prismatic habit, elongated along the lengths of rod modules; and (c) its ∼85°/95° cleavage angles in thin section.

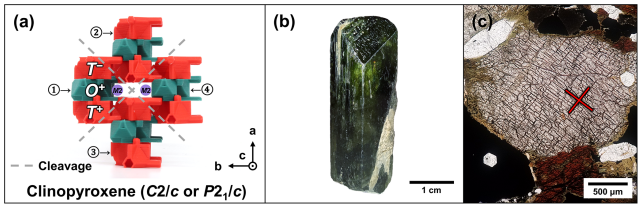

Published by Copernicus Publications on behalf of the European mineralogical societies DMG, SEM, SIMP & SFMC.

1 Introduction and problem statement

Many rock-forming chain and sheet silicate minerals, e.g., pyroxenes, amphiboles, micas, and clay minerals, are built from shared chemical building blocks (Zoltai, 1981; Nespolo and Bouznari, 2017). These rod-like building blocks are known as T-O-T modules because each module consists of two opposing chains of vertex-sharing silica tetrahedra (T), which sandwich a ribbon of edge-sharing metal–oxygen octahedra (O) in a T-O-T configuration (Fig. 1). These modular rock-forming minerals are both abundant and diverse in the lithosphere, accounting for 26 % of the crust and 15–40 % of the upper mantle, as well as representing ∼ 23 % of silicate species (Ronov and Yaroshevsky, 1969; McDonough and Rudnick, 1998; Pasero, 2020; Ralph, 2020). The abundance and diversity of these minerals are due to the chemical and structural versatility of the T and O modules: the modules can accommodate many different ions within their sites (see Sect. S1.1 in File S1 in the Supplement) and can be linked in different ways (Zoltai, 1981; Nespolo and Bouznari, 2017). Due to their abundance and diversity, minerals which are built upon T and O modules are invaluable tools for deciphering geological processes (e.g., Brimhall et al., 1985). However, this versatility leads to the development of complex, 3D crystal structures, which introduces conceptual challenges for both students and geoscientists in solving geological problems (Dyar et al., 2004; Wood et al., 2017).

Conventional visualization methods for mineral structures include physical ball-and-stick models (e.g., Beevers models; Miramodus Ltd. Company, 2021) and computer visualization software (e.g., VESTA; Momma and Izumi, 2011). However, both have limitations. In addition to being expensive (a single model costs between GBP 35–1500; Miramodus Ltd. Company, 2021), ball-and-stick models give a static representation of the entire mineral structure that does not allow individual unit cells or building blocks to be isolated (i.e., disassembly is impractical). In contrast, visualization software is dynamic (the visibility of different features can be toggled), but the interaction is abstract and mediated through a 2D screen. For both methods, recognizing the relationships between different minerals requires a conceptual leap because each structure is represented as a standalone entity. In addition to conventional visualization methods, 3D-printed modular ball-and-stick and space-filling models have been explored in inorganic chemistry (Brown et al., 2019; Rodenbough et al., 2015), but their polyhedral counterparts remain undeveloped. Polyhedral models are commonly used in mineralogy to emphasize the cation sites within the crystal structure, which greatly simplifies the crystal structures in comparison to ball-and-stick models (compare Fig. 1e and f).

Here, we explore how 3D printing can be combined with modular mineralogical theory to illustrate the crystal-structural relationships between rock-forming minerals. The open-source TotBlocks project consists of 3D-printed interlocking brick modules, based on ideal polyhedral representations of T and O rod modules, which can be assembled to illustrate the crystal structures of modular minerals. We use TotBlocks to illustrate the crystal structures of the biopyribole–palysepiole minerals (viz. mica, smectite, pyrophyllite–talc, pyroxene, amphibole, palygorskite, and sepiolite (super-)groups), including non-traditional series members (e.g., clinojimthompsonite, chesterite, and kalifersite), as well as other structurally related, layered minerals (e.g., brucite-, kaolinite–serpentine-, and chlorite-group minerals). We then demonstrate that the configuration of the T-O-T modules within these minerals can be used to accurately derive many mineral properties by first principles, e.g., habit, cleavage angles, and symmetry/polytypism. Finally, we compare 3D-printed, modular, and polyhedral models (TotBlocks) to conventional aids for visualizing crystal structures and explore their wider implications within mineralogy and crystallography.

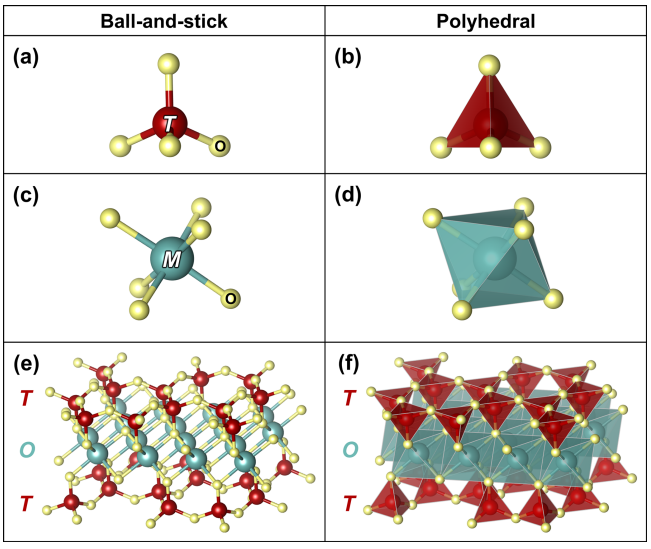

Figure 1. The two key cation sites in modular rock-forming minerals: **(a)** ball-and-stick and **(b)** polyhedral representations of tetrahedrally coordinated T sites, which are occupied primarily by Si, less by Al, and sometimes by Fe^{3+}, with the latter best illustrated in phyllosilicates (Rieder et al., 1998); **(c)** ball-and-stick and **(d)** polyhedral representations of octahedrally coordinated M sites, which are commonly occupied by Fe, Mg, and Al. The ligands (labelled O) are typically occupied by O and lesser OH but can also be occupied by F and Cl. **(e)** Ball-and-stick and **(f)** polyhedral representations of the T-O-T structure found in modular silicate minerals, consisting of chains or sheets of vertex-sharing T sites that sandwich ribbons or sheets of edge-sharing M sites (O). Atomic sites are based on Hendricks and Jefferson (1939) and illustrated using VESTA (Momma and Izumi, 2011).

2 Background

Johannsen (1911) introduced the term "biopyribole" (biotite–pyroxene–amphibole) as a collective field term for chain

and sheet silicates when a more precise identification was not visually possible in the field. The crystal-chemical link between these chain and sheet silicates was proposed by Thompson (1970, 1978), who demonstrated that amphibole-supergroup minerals could be expressed as a combination of modules or "polysomes" derived from pyroxene-group minerals and 2 : 1 phyllosilicates (i.e., mica- and pyrophyllite–talc-group minerals), thus establishing the "biopyribole polysomatic series". Following this approach, Veblen and Burnham (1978a, b) discovered the non-classical biopyriboles, jimthompsonite and clinojimthompsonite, both named in honor of Jim Thompson, as well as chesterite. A similar polysomatic model has been proposed for minerals of the palygorskite and sepiolite groups, known as the "palysepiole polysomatic series" (Ferraris and Gula, 2005), with the proposed crystal structure of kalifersite consisting of alternating palygorskite- and sepiolite-like modules (Ferraris et al., 1998).

Table 1 lists the modular rock-forming minerals, and their structural-chemical formulae are re-written with similar types of cationic sites grouped together (expanded from Thompson, 1978; see Sect. S1.1 for a discussion on the chemical chemistry of modular rock-forming minerals) to emphasize the polysomatic relationships between these minerals, with examples described below (mineral abbreviations from Warr, 2021).

1. Amphibole can be described as the sum of pyroxene and 2 : 1 phyllosilicate modules (Thompson, 1970, 1978):
   $A^{\S}B_2M_5T_8O_{22}(OH)_2$(**Amp**) =
   $B_2M_2T_4O_{12}$(**Px**) + $A^{\S}M_3T_4O_{10}(OH)_2$
   (**2 : 1 phyllosilicate**).

2. Chesterite can be produced from the sum of amphibole and jimthompsonite modules (Thompson, 1978):
   $A^{\S}_3B_4M_{13}T_{20}O_{54}(OH)_6$(**Chs**) =
   $A^{\S}B_2M_5T_8O_{22}(OH)_2$(**Amp**) +
   $A^{\S}_2B_2M_8T_{12}O_{32}(OH)_4$(**Jim**).

3. Chlorite can be written as a 2 : 1 phyllosilicate with alkali interlayer cations (A) being replaced by a brucite module (Thompson, 1978):
   $M_6T_4O_{10}(OH)_8$(**Chl**) = $[M_3(OH)_6]M_3T_4O_{10}(OH)_2$
   ([**Brc**]**2 : 1 phyllosilicate**).

4. The silicate backbone of kalifersite is a combination of those from palygorskite and sepiolite (Ferraris et al., 1998; "[]" denotes omitted sites):
   $[]T_{20}O_{50}(OH)_6$(**Klf**) = $[]T_8O_{20}(OH)_2$(**Plg**) +
   $[]T_{12}O_{30}(OH)_4$(**Sep**).

The biopyribole and palysepiole polysomatic series are intrinsically related to one another because both series are composed of T-O-T modules. Zoltai (1981) proposed a conceptual model for the biopyribole and palysepiole polysomatic series, based on single-chain-width T-O-T rod modules derived from the structure of the 2 : 1 phyllosilicates, which are linked with a specified vertical offset. Nespolo and Bouznari (2017) expanded on this work by demonstrating, through quantitative comparative analysis, that the T-O-T modules of biopyribole and palysepiole minerals are interchangeable, with only marginal deformations. In the unifying model proposed by Nespolo and Bouznari (2017), variable-width T-O-T modules are derived from the prototype structure of the 2 : 1 phyllosilicates and are linked by structure-building symmetry operations, following the concept of tropochemical cell-twinning (Takéuchi, 1997), with extra sites being added to complete the crystal structures, e.g., the $M4$ (B) site in amphiboles.

The widths of the T-O-T rod modules are based on single-width chains (width $w = 1$, length $l = \infty$), double-width chains ($w = 2$, $l = \infty$), triple-width chains ($w = 3$, $l = \infty$), and infinite-width chains (i.e., sheets; $w = \infty$, $l = \infty$) of silica tetrahedra arranged in a *zweier* layout (Fig. 2a, top labels; modified after Zoltai, 1981; Liebau, 1985; bottom labels depict the equivalent notation after Nespolo and Bouznari, 2017; see Sect. S1.2 for a discussion on notation).

The T-O-T rod modules can be connected widthwise via three different configurations, each of which produces a different vertical offset: (1) phyllosilicate-type linkages, characterized by T^+–T^+, O–O, and T^-–T^- linkages, i.e., infinite sheets with no vertical offset (where T^+ and T^- refer to T modules with apical tetrahedra in opposing orientations; Nespolo and Bouznari, 2017; Fig. 2b); (2) pyribole-type linkages, characterized by O–T^+ and T^-–O linkages with a vertical offset of $\sim 2/3$ of the height of a T-O-T rod module (Fig. 2c); and (3) palysepiole-type linkages, characterized by T^-–T^+ linkages with a vertical offset of an entire T-O-T module (Fig. 2d) (modified from Zoltai, 1981; the fourth layer, consisting of interlayer cations, is omitted here). The phyllosilicate-type linkage is approximately equivalent to increasing the unit width of the T and O modules, thus representing a degenerate case for layered minerals. These three linkage types reflect the three broad subdivisions within the biopyribole–palysepiole minerals: (1) the 2 : 1 phyllosilicates, (2) pyribole series, and (3) palysepiole series. In essence, the biopyribole–palysepiole minerals are modulated by two parameters, the module width and linking method.

The 2 : 1 phyllosilicate prototype structure can also be deconstructed into T and O layer modules that can be used to build other layered structures: O (brucite group and gibbsite), T-O (kaolinite–serpentine group), and T-O-T O (chlorite group) (Thompson, 1978). The crystal-structural relationships of the modular rock-forming minerals are summarized in Fig. 3.

3 Materials and methods

TotBlocks are topologically modeled after the 2 : 1 phyllosilicate prototype structure, with interlayer cations (I) removed

Table 1. Relationships between modular rock-forming minerals, chemical formulae, and module widths.

Mineral structure	Reference formula	Homologous formula*	Equivalent sites	w, $T^{\dagger}$, $Z^{\dagger}$
Pyribole series				
Pyroxenes[1]	$2 \times M2M1T_2O_6$	$B_2M_2T_4O_{12}$	$M2 = B$, $M1 = M$	1, $2^{\ddagger}$, $2^{\ddagger}$
Amphiboles[2]	$A^{\S}B_2C_5T_8O_{22}W_2$	$A^{\S}B_2M_5T_8O_{22}(OH)_2$	$C = M$; $W = OH$	2, 4, 5
Clinojimthompsonite[3]	$(Mg,Fe)_{10}Si_{12}O_{32}(OH)_4$	$A^{\S}_2\ B_2M_8T_{12}O_{32}(OH)_4$	$(Mg,Fe)_{10} = B_2M_8$	3, 6, 8
Chesterite[3]	$(Mg,Fe)_{17}Si_{20}O_{54}(OH)_6$	$A^{\S}_3B_4M_{13}T_{20}O_{54}(OH)_6$	$(Mg,Fe)_{17} = B_4M_{13}$	$2 \cdot 3$, $4 \cdot 6$, $5 \cdot 8$
Palysepiole series				
Palygorskite group[4]	$M1M2_2M3_2M4^{\S}_2T_8O_{20}$ $(OH)_2(H_2O,OH)_4 \cdot W$	$A^{\S}B^{\S}_2M_5T_8O_{20}(OH)_2 \cdot nH_2O$	$M1$, $M2$, $M3 = M$; $M4 = B^{\S}$; $W = nH_2O + A^{\S}$	2, 4, 5
Sepiolite group[5]	$Mg_8Si_{12}O_{30}(OH)_4(H_2O)_4 \cdot 8H_2O$	$\{?\}M_8T_{12}O_{30}(OH)_4 \cdot nH_2O$	$Mg = M$	3, 6, 8
Kalifersite[6]	$A_5Y_9Si_{20}O_{50}(OH)_6 \cdot nH_2O$	$A_5M_9T_{20}O_{50}(OH)_6 \cdot nH_2O$	$Y = M$	$2 \cdot 3$, $4 \cdot 6$, $3 \cdot 6$
Layered minerals				
Brucite group[7]	$3 \times Mg(OH)_2$	$M_3(OH)_6$		∞, $-$, $3^{|}$
1 : 1 phyllosilicates[8]	$M_3T_2O_5(OH)_4$	$M_3T_2O_5(OH)_4$		∞, 2, $3^{|}$
2 : 1 phyllosilicates[7]	$\sim I^{\S}M_3T_4O_{10}A_2$	$A^{\S}M_3T_4O_{10}(OH)_2$	$I^{\S} = A^{\S}$; $A = OH$	∞, 2, $3^{|}$
Chlorite group[7]	$0.5 \times M_{12}T_8O_{20}(OH)_{16}$	$M_6T_4O_{10}(OH)_8$		∞, 2, $3^{|}$

"{?}" indicates that extra sites are likely to exist, as indicated by the excess Na in loughlinite (Fahey, 1960). "·" indicates that the structure is a combination of module widths. * Descriptions of cationic site groupings: A = **a**lkali sites which occupy inter-module spaces, B = sites **b**ordering (flanking) O modules, M = **m**etallic sites within O modules, and T = **t**etrahedrally coordinated sites within T modules. Anion sites occupied by OH groups may also accommodate F, O, H_2O, and Cl. See Sect. S1.1 for a detailed description. † T and Z values from Nespolo and Bouznari (2017). ‡ Due to symmetry reasons, the pyroxene module defined in Nespolo and Bouznari (2017) is half of that listed here, in Thompson (1978), and in Zoltai (1981). § Sites can be dominated by vacancies. $^{|}$ Layered structures ($w = \infty$) are equivalent to $Z = 3$ and $T = 2$ modules that are linked by phyllosilicate-type linkages (extrapolated from Nespolo and Bouznari, 2017). References: [1] Morimoto et al. (1988), [2] Hawthorne et al. (2012), [3] Veblen and Burnham (1978b), [4] Leung and McDonald (2020), [5] Brauner and Preisinger (1956), [6] Ferraris et al. (1998), [7] Deer et al. (2013), and [8] Dixon (1989).

from the structure (compare Fig. 4a and c). The T-O-T modules were designed in the open-source, parametric 3D modeling program OpenSCAD version 2021.01 (Kintel, 2021) and are derived from planar sheets of vertex-sharing tetrahedra and edge-sharing octahedra, respectively, with no structural size mismatch between the T and O modules (following the theoretical geometry of Sect. S1.1). In Fig. 4b and d, a single-chain-width module is extracted from the 2 : 1 phyllosilicate structure and displayed in orthographic projection. The component T and O modules are illustrated in Fig. 5 (see Sect. S1.3 for design details). The *.stl files produced by OpenSCAD were subsequently sliced into *.gcode files using PrusaSlicer version 2.3.3 and printed with a Prusa i3 MK3S 3D printer using polylactic acid (PLA) filament (Prusa, 2021).

4 Results

In this section, we explore the relationships between modular rock-forming minerals by providing a systematic overview of their crystal structures using TotBlocks (Fig. 3), including the 2 : 1 phyllosilicates (Sect. 4.1), pyribole series (pyroxene group, amphibole supergroup, clinojimthompsonite, and chesterite; Sect. 4.2), palysepiole series (palygorskite group, sepiolite group, and kalifersite; Sect. 4.3), and other layered minerals (brucite, kaolinite–serpentine, and chlorite groups; Sect. 4.4). The assembly instructions and links to videos for constructing each mineral structure using TotBlocks can be found in File S2 in the Supplement.

The biopyribole–palysepiole minerals also exhibit polytypism due to the variability in the stacking orientations of T-O-T modules (Thompson, 1981). An example of polytypism is presented using the pyroxene structure. For subsequent minerals presented here, the simplest polytype (consisting only of O^{+} modules, i.e., the monoclinic polytype) will be discussed when possible.

4.1 2 : 1 phyllosilicates – mica, smectite, and pyrophyllite–talc groups

The 2 : 1 phyllosilicates (structural formula $\sim IM_3T_4O_{10}A_2$; Rieder et al., 1998; Deer et al., 2013) consist of infinite sheets of T-O-T modules and represent the prototype structure of the modular rock-forming minerals (Fig. 4c). The 2 : 1 phyllosilicates include the mica, smectite, and pyrophyllite–talc groups. These mineral groupings are differentiated by the occupants of the interlayer between T-O-T modules (I, an A-type site; Guggenheim et al., 2006).

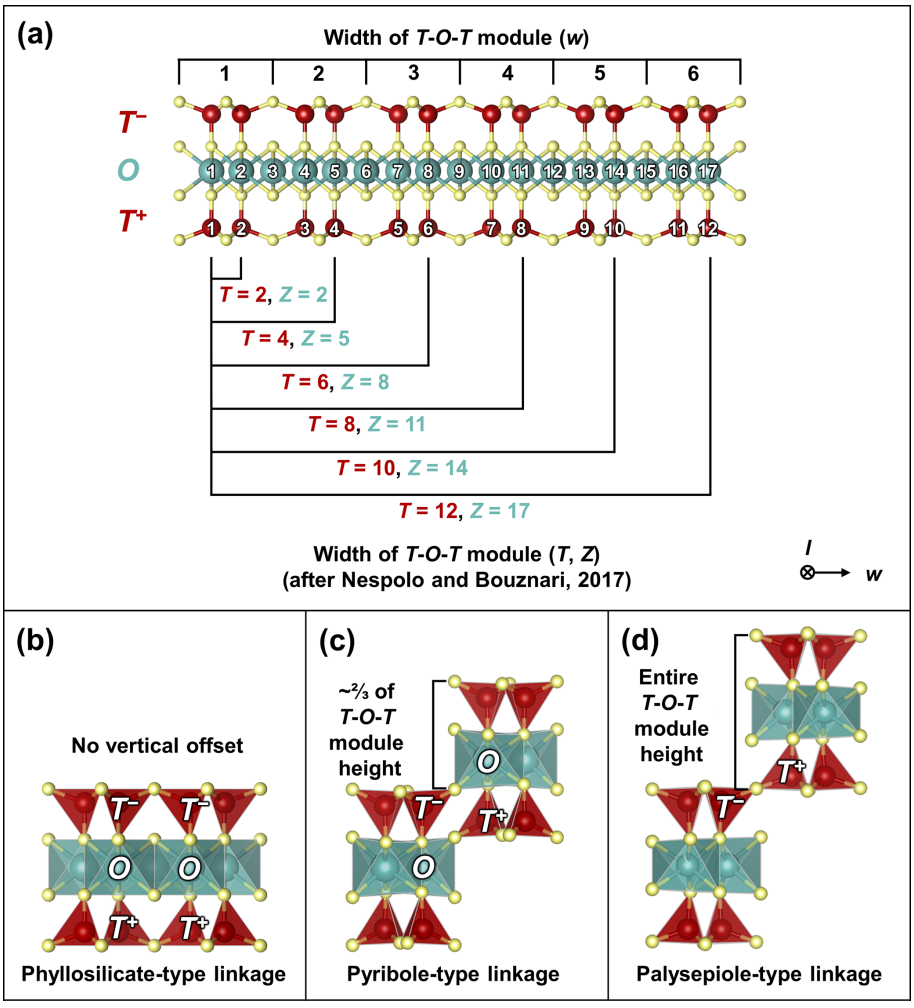

Figure 2. **(a)** Defining the widths of T-O-T modules. The first notation (top labels) describes the number of single-chain-width units (w) that exist within the modules (modified after Zoltai, 1981). The second notation (bottom labels) counts the number of sites (T, Z) that make up the T and O modules (after Nespolo and Bouznari, 2017; note that not all T and Z combinations are shown; see Sect. S1.2 for a discussion). **(b–d)** The three types of linkages for T-O-T modules: **(b)** phyllosilicate-type linkage, showing T^{+}–T^{+}, O–O, and T^{-}–T^{-} linkages (after Hendricks and Jefferson, 1939); **(c)** pyribole-type linkage, showing O–T^{+} and T^{-}–O linkages (after Cameron et al., 1973); **(d)** palysepiole-type linkage, showing T^{-}–T^{+} linkages (after Leung and McDonald, 2020). All crystal structures illustrated using VESTA (Momma and Izumi, 2011). The + and − notation indicates the orientation of the apices.

1. In mica-group minerals, the interlayer is occupied by alkali cations such as K, Na, and Ca (circles labelled I in Fig. 4a and c).

2. In smectite-group minerals, the interlayer is partially occupied by hydrated cations with variable H_2O contents ($\sim I_{0.3–0.7}M_3T_4O_{10}A_2 \cdot nH_2O$). These minerals are also known as swelling or expandable clays because they swell in the presence of H_2O.

3. In pyrophyllite–talc-group minerals, the interlayer is vacant.

4.2 Pyribole series

The pyribole series (Fig. 6) consists of variable-width T-O-T rod modules, which are connected by pyribole-type linkages (T^{-}–O, O–T^{+}; Fig. 2c): pyroxene group ($w = 1$), amphibole supergroup ($w = 2$), clinojimthompsonite ($w = 3$), and chesterite ($w = 2 \cdot 3$). Each structure will be illustrated further in the following sections. In general, pyribole minerals contain an extra site flanking the O modules (B sites; Table 1), which is vertically linked to the T sites of adjacent T-O-T rod modules. For $w > 1$, there are additional spaces between the T-O-T rod modules (A sites; Table 1), which can be vacant or accommodate large alkali cations (e.g., Na, K, and Ca for the amphibole supergroup; Hawthorne et al.,

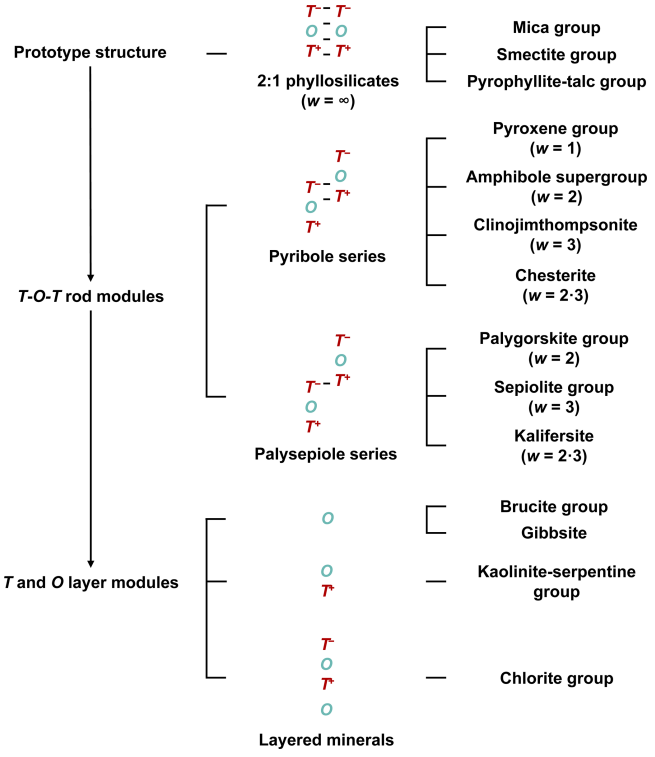

Figure 3. Summary of the crystal-structural relationships between modular minerals that are based on T and O modules. From the 2 : 1 phyllosilicate prototype structure, T-O-T rod modules are extracted widthwise to construct the crystal structures of the pyribole and palysepiole series, whereas T and O layer modules are extracted to construct other layered mineral structures. Visual representations of the linkages can be seen in Fig. 2b–d. "·" indicates that the structures consist of a combination of modules of different widths.

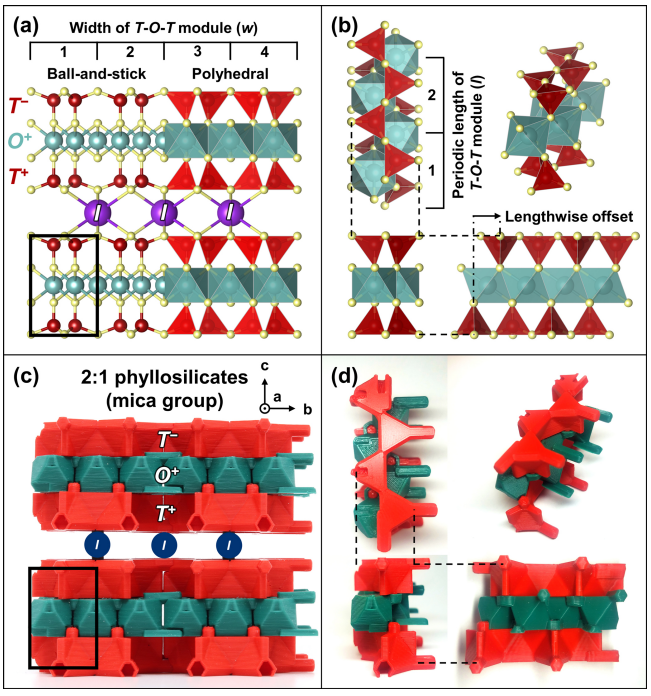

Figure 4. Modeling of TotBlocks after the 2 : 1 phyllosilicate prototype structure. **(a)** Ball-and-stick and polyhedral representations of the crystal structure of the mica group (Hendricks and Jefferson, 1939) using VESTA (Momma and Izumi, 2011). The black rectangle represents the location for a single-chain-width ($w = 1$) T-O-T rod module that is extracted in **(b)**. **(b)** Extraction of the single-width T-O-T rod module (polyhedral representation), displayed as orthographic projections. **(c)** Equivalent structure of the 2 : 1 phyllosilicates using TotBlocks (black pegs are structural supports intended to hold individual layers; the positions for missing interlayer sites I are labelled circles). **(d)** Equivalent single-chain-width ($w = 1$) T-O-T rod module using TotBlocks, displayed as orthographic projections.

2012). Minerals of the pyribole series account for a significant proportion of the chain silicate (inosilicate) subclass.

4.2.1 Pyroxene group ($w = 1$)

The pyroxene group (structural formula $M2M1T_2O_6$; Morimoto et al., 1988) consists of single chains of T-O-T rod modules that are linked by pyribole-type linkages (Fig. 6a–c). An additional B-type site ($M2$) occupies the spaces between the T-O-T modules. The possible stacking variations of the single chains (specifically O^+ versus O^- modules) produce polytype structures. Three main pyroxene polytypes (sensu lato) are produced by the stacking of O^+ and O^- modules (Thompson, 1981): clinopyroxene (polytype pyroxene-*Mabc*; space-group type $C2/c$ or $P2_1/c$), orthopyroxene (polytype pyroxene-*O2abc*; space-group type *Pbca*), and protopyroxene (polytype pyroxene-*Oabc*; space-group type *Pbcn*) (Bailey et al., 1977; Morimoto et al., 1988).

In summary, clinopyroxenes only use O^+ modules (stacking sequence $++++$; Fig. 6a), whereas orthopyroxenes should show corrugated layers alternating between O^+ and O^- modules (stacking sequence $++--$; Fig. 6b) and protopyroxenes should show alternating, isolated O^+ and O^- modules (stacking sequence $+-+-$; Fig. 6c). The O^+ modules in the clinopyroxene structure lead to a horizontal, lengthwise stacking offset and monoclinic symmetry, whereas the alternating O^+ and O^- modules negate the stacking offset in both orthopyroxene and protopyroxene structures, leading to orthorhombic symmetry (see Sect. 5.1.3 for a discussion on polytypes and symmetry).

4.2.2 Amphibole supergroup ($w = 2$)

The amphibole supergroup (structural formula $AB_2C_5T_8O_{22}W_2$; Hawthorne et al., 2012) consists of double chains of T-O-T rod modules that are linked by pyribole-type linkages (Fig. 6d). Additional sites occupy the spaces between and flank the T-O-T rod modules (A and B sites, respectively).

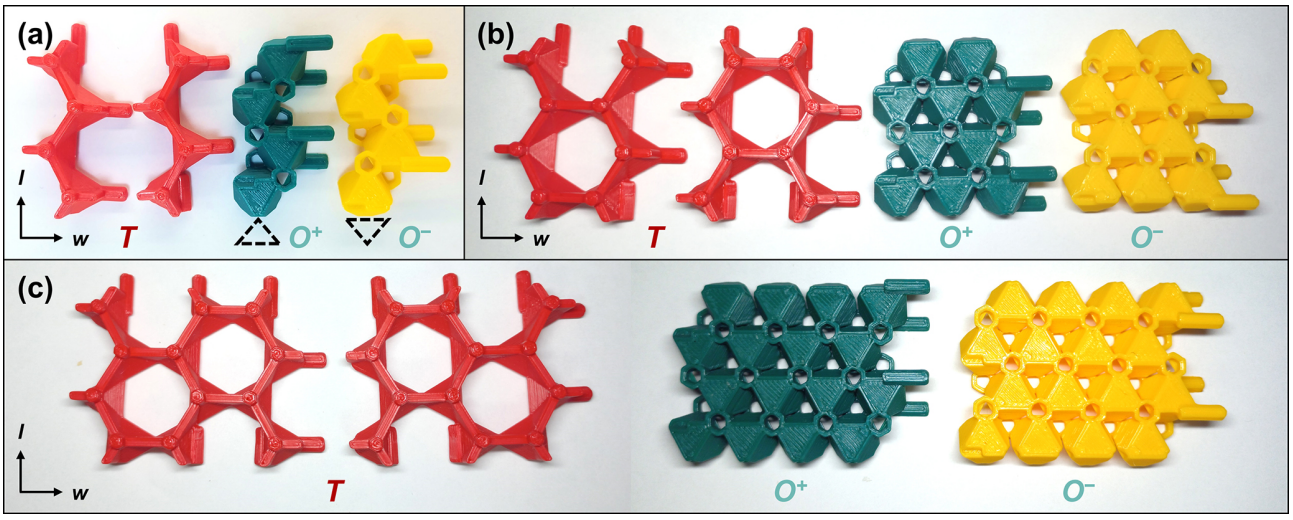

Figure 5. The four types of T and O modules for **(a)** single-chain ($w = 1$), **(b)** double-chain ($w = 2$), and **(c)** triple-chain ($w = 3$) T-O-T rod modules. Note that the two variations of T modules are interchangeable, and the T^+ and T^- designation relates only to the direction that the apices of the T modules are pointing (up and down, respectively). See Sect. S1.3 for ancillary components of TotBlocks.

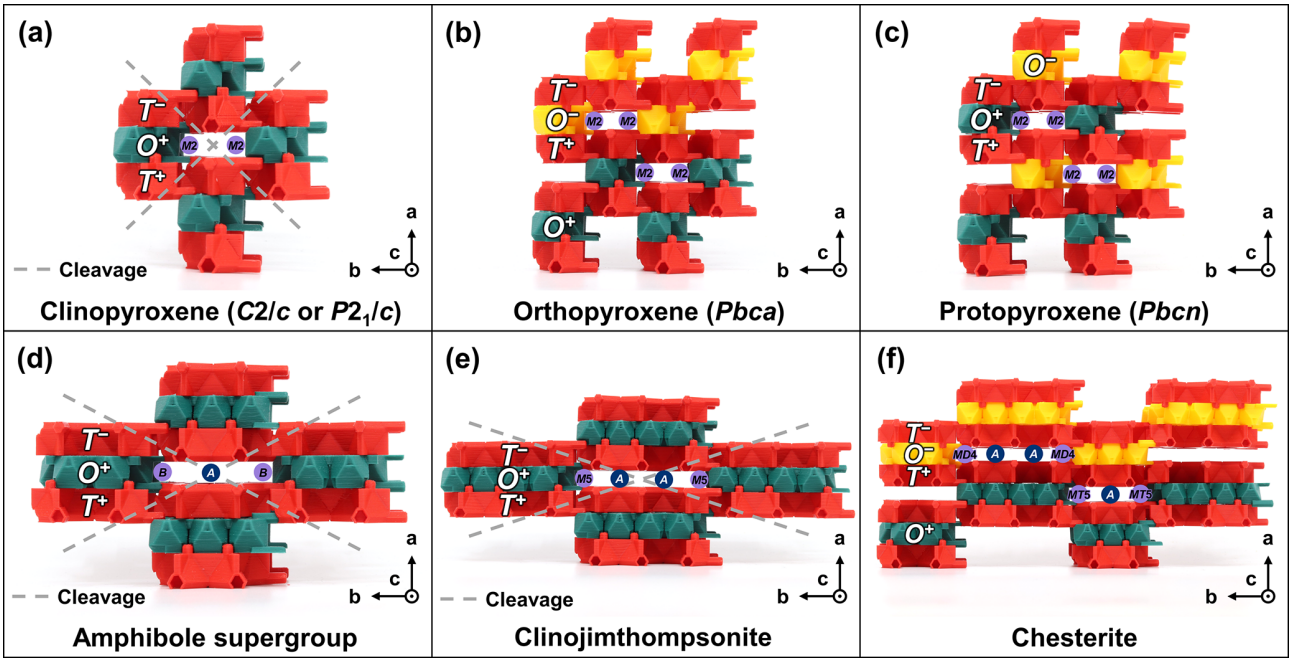

Figure 6. TotBlocks representations of the pyribole series. The T and O modules, as well as circles indicating the locations of additional sites that occupy the spaces between the T-O-T modules, are labelled. **(a–c)** Polytypes of pyroxenes ($w = 1$): **(a)** clinopyroxene (e.g., Cameron et al., 1973), **(b)** orthopyroxene (e.g., Carlson et al., 1988), **(c)** protopyroxene (e.g., Jahn and Martonak, 2009), **(d)** amphibole supergroup (e.g., Fischer, 1966), **(e)** clinojimthompsonite, and **(f)** chesterite (Veblen and Burnham, 1978a, b).

4.2.3 Clinojimthompsonite ($w = 3$)

Clinojimthompsonite ($(Mg,Fe)_{10}Si_{12}O_{32}(OH)_4$; Veblen and Burnham, 1978a) consists of triple chains of T-O-T rod modules that are linked by pyribole-type linkages (Fig. 6e). An additional B-type site ($M5$) is located at the boundary of the O module, which vertically links to the T sites in adjacent T-O-T rod modules (not shown). Trace amounts of Na are incorporated in A-type sites, which are otherwise vacant (Veblen and Burnham, 1978a; labelled as A in Fig. 6e).

4.2.4 Chesterite ($w = 2 \cdot 3$)

Chesterite ($(Mg,Fe)_{17}Si_{20}O_{54}(OH)_6$; Veblen and Burnham, 1978a) consists of alternating double and triple chains of *T*-*O*-*T* rod modules that are linked by pyribole-type linkages (Fig. 6f). Like other pyribole-series minerals, there are additional *B* sites (*MD*4 and *MT*5) at the edges of the *O* modules, which vertically link to the *T* sites in adjacent *T*-*O*-*T* rod modules. *A*-type sites are dominantly vacant but likely incorporate trace Na (Veblen and Burnham, 1978a; labelled as *A* in Fig. 6f).

4.3 Palysepiole series

The palysepiole series (Fig. 7a–c) consists of variable-width *T*-*O*-*T* modules which are connected by palysepiole-type linkages (T^+–T^-; Fig. 2d): palygorskite group ($w = 2$), sepiolite group ($w = 3$), and kalifersite ($w = 2 \cdot 3$). The palysepiole-type linkage produces a vertical offset of one *T*-*O*-*T* module, which produces large channels that are commonly filled with H_2O (and more rarely, octahedrally coordinated *A*-type sites; Table 1; Ferraris et al., 1998; Pluth et al., 1997). A consequence of this linkage is that the edges of *O* modules are not cross-linked to other *T*-*O*-*T* rod modules and thus must rely on bonds with structurally bound H_2O groups. Interestingly, a sensu stricto $w = 1$ member of the palysepiole series is not known to exist in nature, potentially due to the instability of the narrow channels within which H_2O groups cannot fit, although broadly similar structures exist (see Sects. 5.3 and S1.5.2 for brief discussions). Minerals of the palysepiole series are typically classified under clay minerals or modulated 2 : 1 phyllosilicates.

4.3.1 Palygorskite group ($w = 2$)

The palygorskite group (structural formula $M1M2_2M3_2M4_2T_8O_{20}(OH)_2(H_2O,OH)_4 \cdot W$; Leung and McDonald, 2020) consists of double chains of *T*-*O*-*T* rod modules, which are linked by palysepiole-type linkages (Fig. 7a). Three regular octahedral sites (*M*1, *M*2, and *M*3) are located within the *O* module (see Fig. S1.5b for the locations of the octahedral sites within the *O* module). In palygorskite and windmountainite, the *M*1 site is vacant, resulting in an intermediate dioctahedral–trioctahedral *O* module (Leung and McDonald, 2020). Extra sites include (1) a distorted and dominantly vacant, octahedral site (*M*4, a *B*-type site; Table 1), which borders the *O* rod module, and (2) H_2O groups (*W* in the structural formula), which occupy the channel spaces between the *T*-*O*-*T* modules (labelled *M*4 and nH_2O in Fig. 7a). In raite, $Mn^{2+}Mn_2^{2+}Na_2(\square,Ti)_2Si_8O_{20}(OH)_2(H_2O)_4 \cdot Na(H_2O)_6$, there is an additional *A*-type site occupied by Na (Pluth et al., 1997; Leung and McDonald, 2020; labelled as *A* in Fig. 7a).

4.3.2 Sepiolite group ($w = 3$)

The sepiolite group (i.e., minerals isostructural to sepiolite, $Mg_8Si_{12}O_{30}(OH)_4(H_2O)_4 \cdot 8H_2O$; Brauner and Preisinger, 1956) consists of triple chains of *T*-*O*-*T* rod modules which are linked by palysepiole-type linkages (Fig. 7b). The channels are occupied by H_2O groups (not shown). The presence of two extra Na cations in loughlinite, $Na_4Mg_6Si_{12}O_{32} \cdot 16H_2O$, suggests that extra *A*- or *B*-type sites exist within the channels of sepiolite-group minerals, although the crystal structure of loughlinite has not been refined (Fahey et al., 1960). Additionally, sepiolite crystallizes in the orthorhombic system with the space-group type *Pnan* and, at the time of writing, the monoclinic polytype has not been recognized in the literature. Thus, both O^+ and O^- modules are used to construct the crystal structure of sepiolite.

4.3.3 Kalifersite ($w = 2 \cdot 3$)

The crystal structure of kalifersite $((K,Na)_5(Fe^{3+},\square)_9Si_{20}O_{50}(OH)_6 \cdot 12H_2O$; Ferraris et al., 1998) can be considered as alternating double ($w = 2$) and triple chains ($w = 3$) of *T*-*O*-*T* rod modules, which are linked by palysepiole-type linkages, or in other words, is a combination of palygorskite-like and sepiolite-like modules (Fig. 7c). However, the *O* modules of both types are missing an octahedral site (of double multiplicity) on the edge of the *O* modules, yielding Z_3 and Z_6 rod modules (Fig. S1.4) instead of the typical Z_5 and Z_8 modules found in palygorskite and sepiolite, respectively (Nespolo and Bouznari, 2017). The channels between the *T*-*O*-*T* rod modules are occupied by five $(K, Na)(H_2O)_6$ sites (labelled *A* in Fig. 7c).

4.4 Modular minerals based on *T* and *O* layer modules

Beyond the rod modules of the biopyribole–palysepiole series, the 2 : 1 phyllosilicate structure can also be deconstructed into *T* and *O* layer modules that are stacked vertically to produce layered minerals: brucite group and gibbsite (*O*), kaolinite–serpentine group (*T*-*O*), and chlorite group (*T*-*O*-*T* *O*). Like the 2 : 1 phyllosillicate structure, these layered mineral structures also exhibit polytypism by changing the orientations of the vertically repeated modules.

4.4.1 Brucite group and gibbsite (*O*)

Brucite, $Mg(OH)_2$, and related minerals (general structural formula of $\sim M_3(OH)_6$) consist of *O* layer modules (i.e., trioctahedral sheets of edge-sharing $M(OH)_6$ octahedra) that are vertically linked by hydrogen bonds (Fig. 7d; Deer et al., 2013). Gibbsite, $Al(OH)_3$, represents the dioctahedral equivalent of brucite (Deer et al., 2013).

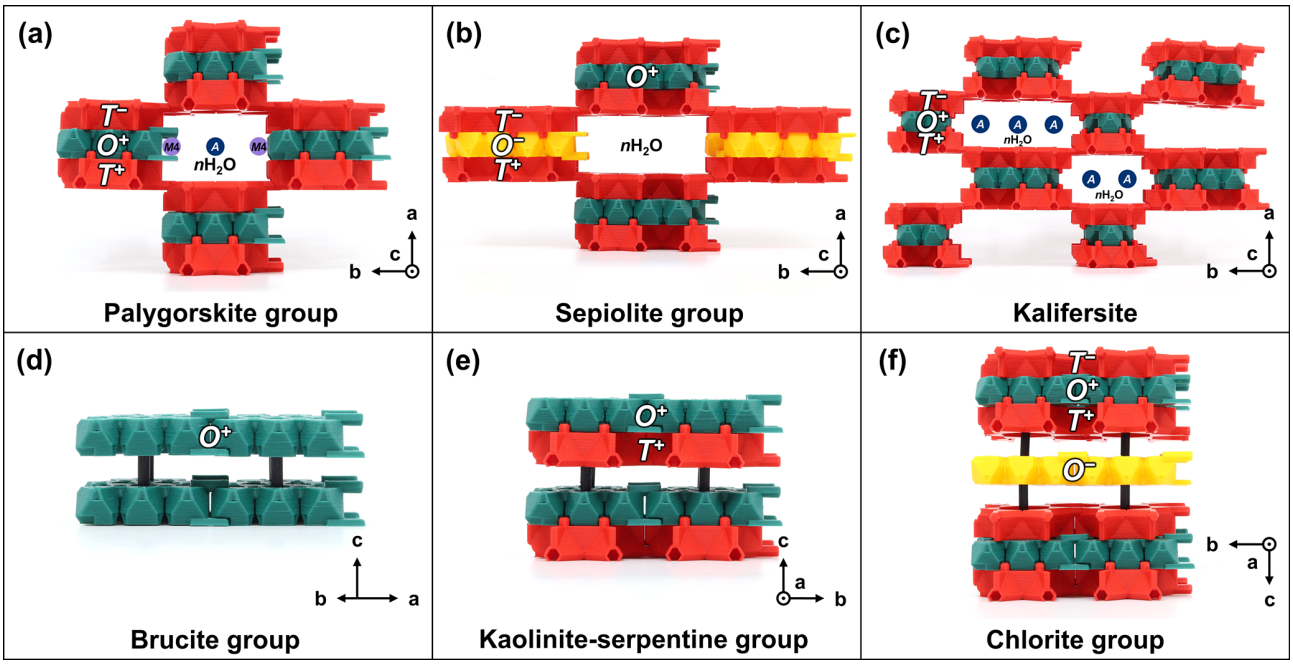

Figure 7. TotBlocks representations of the palysepiole series and other layered minerals: **(a)** palygorskite group (e.g., Leung and McDonald, 2020), **(b)** sepiolite group (e.g., Post et al., 2007), **(c)** kalifersite (Ferraris et al., 1998), **(d)** brucite group (e.g., Nagai et al., 2000), **(e)** lizardite (kaolinite–serpentine group; Mellini, 1982), and **(f)** chlorite group (Zanazzi et al., 2007). Additional sites are denoted by labelled circles (see main text). Black pegs are structural supports intended to hold individual layers; see Fig. S1.3b.

4.4.2 Kaolinite–serpentine group (1 : 1 phyllosilicates; *T*-*O*)

The kaolinite–serpentine group (structural formula $M_3Si_2O_5(OH)_4$; Dixon, 1989) consists of T-O layer or rod modules. The Mg-rich serpentines consist of three main polymorphs: lizardite (Fig. 7e), chrysotile, and antigorite (Demichelis et al., 2016). In lizardite (Fig. 7e), the T-O modules form continuous planar layers, whereas the size mismatch between the T and O modules in chrysotile leads to chrysotile adopting a convex structure that coils on itself, resulting in a fibrous, asbestiform habit. Antigorite consists of T-O rod modules that are modulated lengthwise (as opposed to the widthwise modulation found in most biopyribole–palysepiole minerals) and are connected by O–O and T^+–T^- linkages, leading to a platy, striated habit. The structure of antigorite (polysome $m = 16$) would be built using $l = 4$ T-O modules which connect lengthwise by joining T^+ and T^- modules together (crystal structure not shown here; Capitani and Mellini, 2006). Kaolinite, $Al_2Si_2O_5(OH)_4$, represents the dioctahedral equivalent of lizardite, $Mg_3Si_2O_5(OH)_4$ (Dixon, 1989).

4.4.3 Chlorite group (*T*-*O*-*T* *O*)

The crystal structure of the chlorite group (structural formula $M_{12}T_8O_{20}(OH)_{16}$; Deer et al., 2013) consists of T-O-T layer modules alternating with O layer modules, which are vertically linked by hydrogen bonds (Fig. 7f). Both O layer modules can be dioctahedral or trioctahedral, although no minerals have been described with a combination of trioctahedral T-O-T and dioctahedral O layers (Bailey, 1980).

5 Discussion

5.1 Relationships between physical properties and mineral structures

Using modular, 3D printed, and polyhedral models emphasizes the importance of the T-O-T module present in the modular rock-forming minerals (e.g., Deer et al., 2013), which is central to making comparisons between these minerals. For example, pyroxenes (Fig. 6a–c) and amphiboles (Fig. 6d) are similar because their T-O-T modules are linked in the same way, but they are distinguished by the width of the T-O-T modules (single versus double chains). Conversely, the crystal structures of amphiboles (Fig. 6d) and palygorskite-group minerals (Fig. 7a) share T-O-T modules of equal widths, but they differ in terms of how the modules are linked (pyribole versus palysepiole linkages). Comparing the structures of different minerals allows for a better understanding of the variations of their physical properties, which are considered below.

5.1.1 Habit

Mineral habits are ultimately determined at the atomic scale by their crystal structures. Minerals typically grow faster in the direction of strong bonds, as compared to weak bonds (periodic bond-chain theory; Hartman and Perdok, 1955). Thus, periodic bond-chain theory predicts the habits of (1) layered minerals, (2) pyribole-series minerals, and (3) palysepiole-series minerals, based on the configuration of T-O-T modules (Fig. 8).

1. Layered minerals of the brucite, kaolinite–serpentine, pyrophyllite–talc, smectite, mica, and chlorite groups consist of strongly bound layers that are weakly held in the vertical direction, thus exhibiting platy habits (Fig. 8a–b).

2. Pyribole-series minerals, which consist of chains of silica tetrahedra, tend to form prismatic to acicular crystals that extend along the length of the chains (along the crystallographic axis c; Fig. 8c–d).

3. The T^-–T^+ linkages in palysepiole-series minerals are generally unfavorable because they result in strained, Si–O–Si bond angles of 180° (Leung and McDonald, 2020). This leads to macroscopic crystals developing fibrous to acicular habits extending along the lengths of the modules (along the crystallographic axis c; Fig. 8e) or the development of mineral aggregates when the growth of macrocrystals is inhibited (Fig. 8f).

5.1.2 Cleavage

The linkages between T-O-T modules also dictate the cleavage of modular silicate minerals because the linkages between individual T-O-T modules are weaker than the bonds within the modules. The monoclinic pyriboles have two cleavages on the {110} set of planes, and the two supplementary angles between the cleavages diverge from perpendicular with an increase in the module size. The cleavage angles predicted by idealized T-O-T modules are consistent with observed cleavage angles of biopyriboles using crystallographic data (Fig. 9a–d; see Sect. S1.4 for calculations and further comments). The cleavage planes in palysepiole-series minerals are inconsistently described in the literature (e.g., Leung and McDonald, 2020) and thus are not discussed here.

5.1.3 Polytypes and symmetry

Many of the modular rock-forming minerals can exhibit variations in symmetry. These variations in symmetry are a direct result of the T-O-T modules and how they are stacked, i.e., polytypism. The O modules produce a horizontal, lengthwise offset between the adjoined T^+ and T^- modules (Fig. 2b). This offset results in the pseudohexagonal symmetry of mica-group minerals, as opposed to strictly hexagonal symmetry. For pyribole- and palysepiole-series members, the types of O modules used will influence the final symmetry of the mineral. If only O^+ modules are used in the structure, this horizontal offset results in the systematic shifting of the unit cell, resulting in monoclinic symmetry, e.g., in the structure of clinopyroxene (Fig. 10a). However, alternating O^+ and O^- modules negate the horizontal offset, leading to orthorhombic symmetry, as is the case for orthopyroxenes and protopyroxenes (Fig. 10b and c, respectively; Thompson, 1981). The difference in symmetry between pyroxene polytypes manifests as a distinguishing optical property: when viewed parallel to the crystallographic axis b in cross-polarized light, clinopyroxenes exhibit inclined extinction, whereas orthopyroxenes exhibit straight extinction. TotBlocks can also aid in learning about the space-group types of various minerals by considering the symmetry and stacking operations involving T-O-T modules.

5.2 Comparison to conventional teaching aids

TotBlocks are widely accessible due to their low cost, modularity, and open-source nature. Although producing the modules for TotBlocks is currently dependent on a user's access to a 3D printer, these resources are becoming more common in libraries and other makerspaces (Jones et al., 2011; Moorefield and Lang, 2014; Pryor, 2014; Prato and Britton, 2016). Once the initial investment in 3D printing technology has been made, producing additional T and O modules becomes an efficient and cost-effective option. Conversely, physical ball-and-stick models are expensive (e.g., Miramodus Ltd. Company, 2021), and individual models can only visualize a single crystal structure. This situation effectively prices out individual users and reduces the accessibility of these physical manipulatives. TotBlocks proves more accessible because multiple crystal structures can be constructed from the same set of T and O modules. The modular aspect of TotBlocks allows modular rock-forming minerals to be visualized as hierarchical systems decomposed into smaller, interrelated subsystems (T and O modules) that can be variably arranged to account for complexity (Simon, 1962). Although visualization software is free and dynamic (able to visualize multiple structures), the infrastructure required to support virtual manipulatives (e.g., computers, internet, and possibly virtual reality headsets) may pose as an access barrier. In contrast, TotBlocks modules require no support infrastructure. Finally, the open-source nature of TotBlocks allows educators and researchers to freely customize the designs for other interactive uses.

Additionally, TotBlocks promises improvements in interactivity in comparison with traditional ball-and-stick models and visualization software. Where traditional ball-and-stick models are static (a single model can only ever represent the crystal structure of a single mineral), the modularity of TotBlocks allows a variety of mineral structures to be constructed with a single set of modules. The literal sharing of

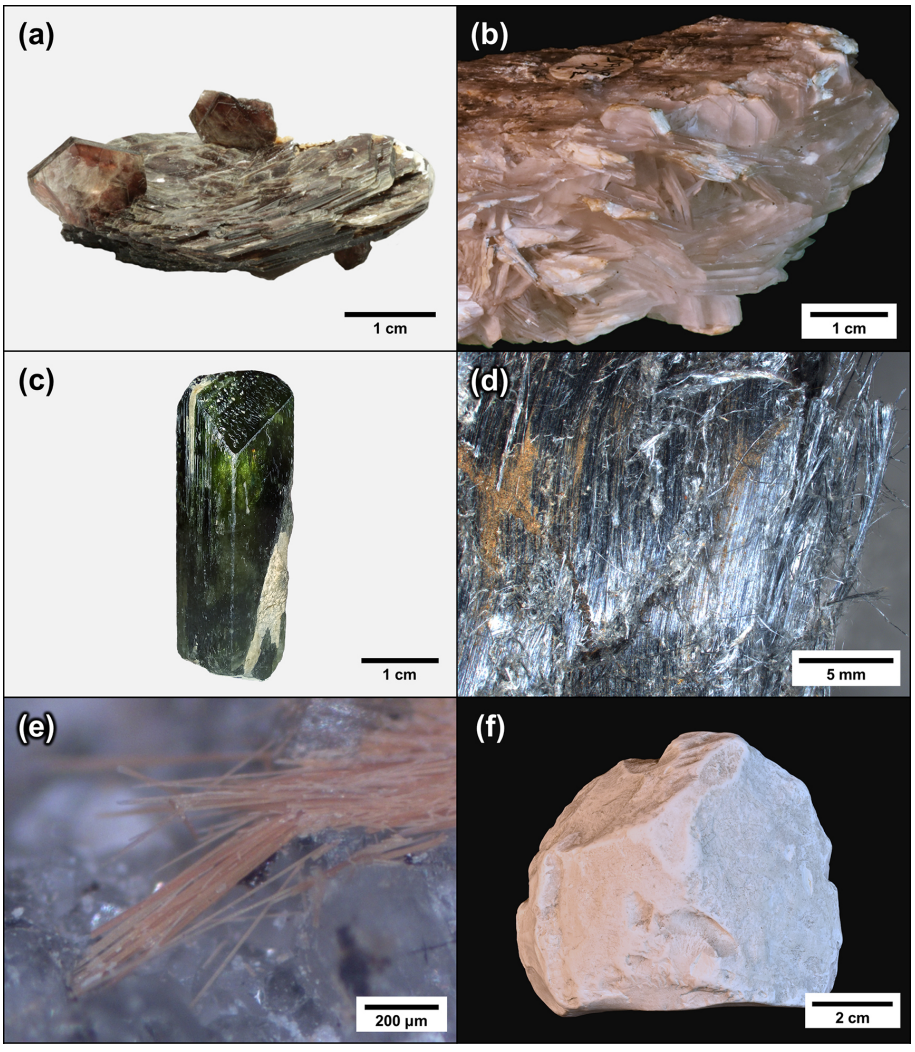

Figure 8. Habits of modular rock-forming minerals. Layered minerals **(a)** muscovite (mica group) and **(b)** brucite typically form platy habits due to the planar nature of T-O-T layer modules. Pyribole-series minerals typically form **(c)** stubby to prismatic (diopside, pyroxene group) and **(d)** acicular to asbestiform (riebeckite var. crocidolite, amphibole supergroup) habits elongated on the crystallographic axis c, which reflects the linear nature of T-O-T rod modules. The highly strained T^{-}–T^{+} linkages in palysepiole-series minerals lead to **(e)** acicular habits (windmountainite, palygorskite group) elongated on the crystallographic axis c and **(f)** mineral aggregates where the growth of macrocrystals is inhibited (sepiolite).

these building blocks elucidates the overarching similarities that unite these structures, as well as the specific changes which mark the differences between these structures. In contrast with computer visualization software such as VESTA (Momma and Izumi, 2011) and those of the Virtual Museum of Minerals and Molecules (Barak and Nater, 2005), TotBlocks place the building blocks of minerals in students' hands and allow them to engage directly and actively in the assembly process. However, computer visualizations retain some advantages over TotBlocks because individual atoms, silica tetrahedra, and the unit cells of crystals can be dynamically highlighted. Ultimately, TotBlocks may prove most effective for communicating mineralogical concepts when integrated with existing visualization resources. This strategy would provide students and researchers with multiple representations of the same system to support their understanding (Fig. 11; Tsui and Treagust, 2013).

5.3 Future directions

The TotBlocks project provides a novel teaching aid for visualizing the crystal structures of modular rock-forming minerals, and supplements existing physical and virtual resources. However, there are still aspects that can be improved. The original morphology of the T sites is obscured by the padding of the T module in single-extrusion models, although this is somewhat rectified by dual extrusion with transparent filament (Fig. S1.5). In terms of crystal chemistry, certain sites

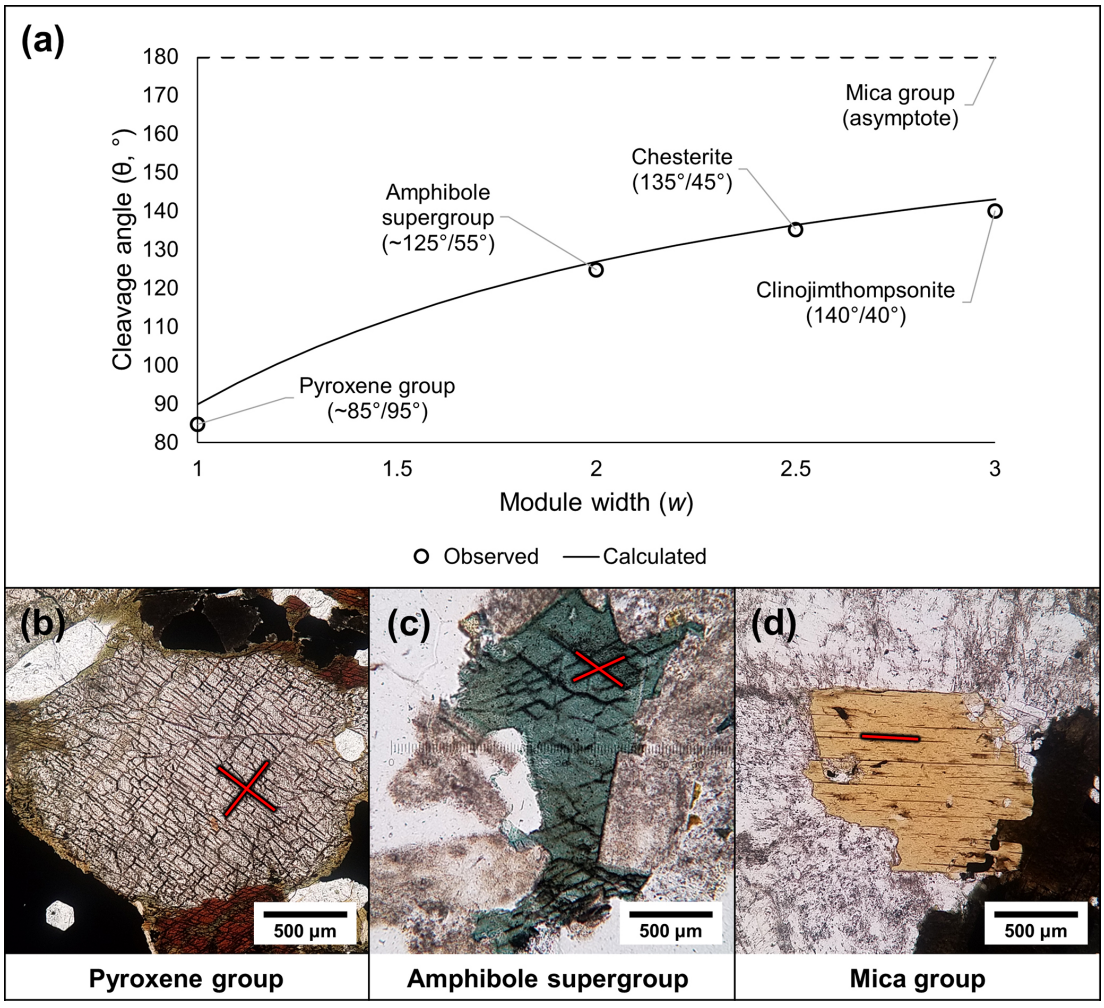

Figure 9. Cleavage angles of the biopyriboles. **(a)** The observed and calculated cleavage angles (see Sect. S1.4) show strong correlation. **(b–d)** Plane-polarized light photomicrographs of biopyribole minerals, showing typical cleavages: **(b)** pyroxene group (∼ 85°/95°; compare with Fig. 6a), **(c)** amphibole supergroup (∼ 125°/55°; compare with Fig. 6d), and **(d)** mica group (one basal cleavage, i.e., 180°/0°; compare with Fig. 4c).

are currently excluded using TotBlocks (e.g., the *B* and *A* types of sites; Table 1) because these sites are not part of the shared *T*-*O*-*T* modules which link the modular minerals and because the shape of these sites varies depending on the configuration of *T*-*O*-*T* modules. Such additions will provide even more insight into the comparisons between different mineral structures (see Sect. S1.5.1 for an extended discussion).

There are still mineral structures yet to be explored using the concept of 3D-printed modular structures, e.g., antigorite, silinaite, pentagonite, and hexacelsian (see Sect. S1.5.2 for an extended dialogue). Moreover, the concept of representing modular mineral series using 3D-printed brick modules can be applied to other modular series such as the heterophyllosilicates, pyroxene–pyroxenoid polysomatic series, and humite–leucophoenicite homologous series (Ferraris and Gula, 2005; Angel and Burnham, 1991; Thompson et al., 2016; Thompson, 1978; Ferraris et al., 2008).

Additionally, the concept of 3D-printed polyhedral models can be customized for the crystal structures of non-modular minerals and other inorganic crystalline substances, e.g., quartz, which is based on repeating modules of three-fold screws of silica tetrahedra (Fig. S1.6). However, the designs for TotBlocks have been produced specifically for biopyribole–palysepiole minerals. As a result, new crystal structures must be designed manually, so the ability for mass customization is limited at the time of writing. At the time of writing, the crystal structure visualization software VESTA (Momma and Izumi, 2011) can export *.stl files for polyhedral crystal structures, but these cannot be directly 3D printed because the polyhedra are joined by the edge or vertex, and the files commonly contain mesh errors that inhibit post-processing. In the future, a computer program should

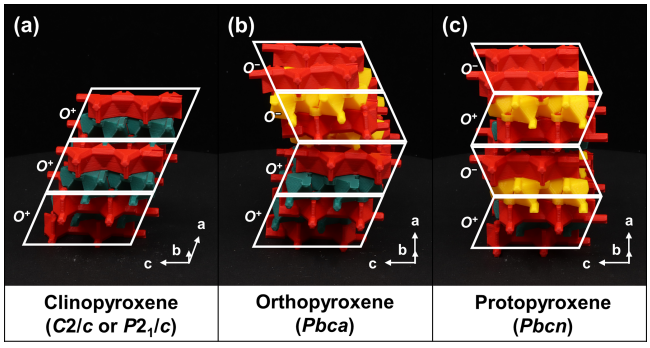

Figure 10. The relationship between polytypes and symmetry for the pyroxene group (Thompson, 1981). The O module produces a stacking offset between the T^+ and T^- modules. **(a)** In the structure of clinopyroxenes, the stacking offset propagates $(++++)$, leading to monoclinic symmetry. **(b)** In orthopyroxenes, the stacking offset alternates for each corrugated layer $(++--)$, resulting in no net offset and orthorhombic symmetry. **(c)** In protopyroxenes, the stacking offset alternates every layer $(+-+-)$, resulting in no net offset and orthorhombic symmetry. Note the departure from Thompson's (1981) notation; see Sect. S1.3.

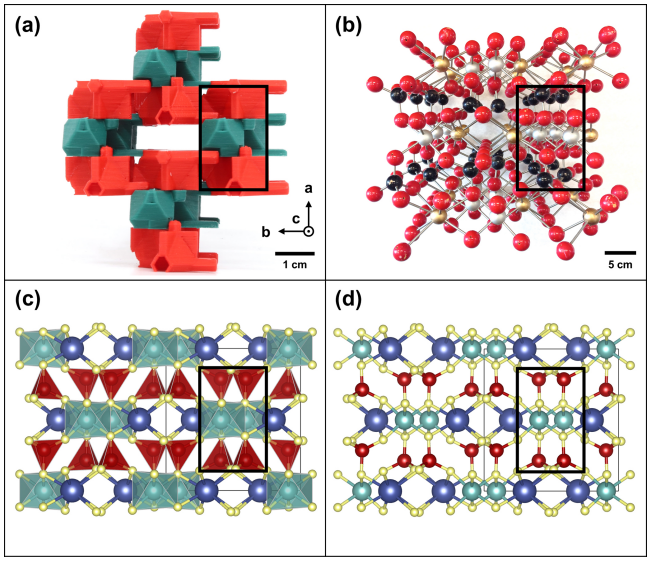

Figure 11. Comparison of the different representations of the crystal structure of diopside (Cameron et al., 1973), a member of the clinopyroxenes, looking down the c axis: **(a)** TotBlocks (photographed), **(b)** physical ball-and-stick models (photographed), and **(c)–(d)** virtual polyhedral and ball-and-stick models rendered using the visualization software VESTA (Momma and Izumi, 2011). Note that the structures are approximately equivalent (solid black rectangles highlight a single-chain-width T-O-T module); the scale bar denotes the actual sizes of the models.

be developed to systematically generate 3D-printable crystal structures. Despite the current limitations with respect to customization, TotBlocks represent a first step toward generating 3D-printed polyhedral components of mineral structures.

6 Conclusions

1. The free and open-source TotBlocks project consists of a novel series of 3D-printed, T-O-T interlocking bricks, based on polyhedral representations of T and O modules, which can be linked via hexagonal pegs and slots. TotBlocks can be used to communicate the crystal structures of the biopyribole and palysepiole series (mica, smectite, pyrophyllite–talc, pyroxene, amphibole, palygorskite, and sepiolite (super-)groups), as well as other related layered minerals (brucite, kaolinite–serpentine, and chlorite groups).

2. TotBlocks can be used to derive the properties of minerals from first principles (e.g., habit, cleavage angles, and symmetry/polytypism) using the configuration of T-O-T modules. These models can supplement existing teaching and outreach aids such as ball-and-stick models and computer visualization software.

3. The combination of 3D printing and modular mineralogical theory yields a widely accessible (open-source models, low overhead printing cost) and interactive (allowing students and researchers to construct and manipulate physical models of mineral structures) solution to communicating the complex crystal structures of common rock-forming minerals.

Code and data availability. The full source code and 3D model files for the TotBlocks project (GPLv3 license) can be found on Zenodo: https://doi.org/10.5281/zenodo.5240816 (Leung, 2022).

Supplement. File S1 contains all supplemental sections and figures referred in the main text (Sect. S1.X.X; Fig. S1.X). Descriptions for Videos S1–S13 can be found in File S1. File S2 contains the assembly instructions for all models described in this contribution. The supplement related to this article is available online at: https://doi.org/10.5194/ejm-34-523-2022-supplement.

Author contributions. DDVL is the lead author of this work, while PEdP is a supporting author. DDVL conceptualized, designed, and 3D printed TotBlocks prototypes; described the crystal structures of chain and sheet silicates; and wrote the first draft of the manuscript. PEdP wrote the instructions for constructing biopyribole–palysepiole minerals using TotBlocks (Supplemental File 2). Both authors photographed mineral specimens and discussed and contributed to the final manuscript.

Competing interests. Derek D. V. Leung holds the copyright for the TotBlocks design files and source code, but these are distributed under a copyleft, open-source license (GPLv3) that is freely available to the public.

Disclaimer. Publisher's note: Copernicus Publications remains neutral with regard to jurisdictional claims in published maps and institutional affiliations.

Acknowledgements. Early prototypes of TotBlocks were designed at the UCreate Studio makerspace at the University of Edinburgh; Mike Boyd, Anthony Middleton, and countless other staff are thanked for their support and encouragement. Access to mineral specimens was provided by Gillian McCay (Cockburn Museum, EUCM), Andrew McDonald, and Irwin Kennedy (HES Mineral Research Collection, Laurentian University). Godfrey Fitton, Geoffrey Bromiley, Tetsuya Komabayashi (University of Edinburgh), and Andrew McDonald (Laurentian University) are thanked for discussing the potential teaching applications of TotBlocks. An image of Jim Thompson used in Video S6 was graciously provided by Louisa Van Baalen. Teddie Leung spent countless hours listening to Derek D. V. Leung ramble on about crystal structures. Kristine Nymoen and Shalaila Bhalla gave feedback on a previous version of the manuscript. Hannah Rogers encouraged the authors to publish the results of this publication. We thank Giovanni Ferraris and an anonymous reviewer for their constructive and supportive comments. We also thank Massimo Nespolo and Sergey Krivovichev for their editorial handling of the manuscript.

Review statement. This paper was edited by Massimo Nespolo and reviewed by Giovanni Ferraris and one anonymous referee.

References

Angel, R. J. and Burnham, C. W.: Pyroxene-pyroxenoid polysomatism revisited: A clarification, Am. Mineral., 76, 900–903, 1991.

Bailey, S. W.: Summary of recommendations of AIPEA nomenclature committee on clay minerals, Am. Mineral., 65, 1–7, 1980.

Bailey, S. W., Frank-Kamenetskii, V. A., Goldztaub, S., Kato, A., Pabst, A., Schulz, H., Taylor, H. F. W., Fleischer, M., and Wilson, A. J. C.: Report of IMA–IUCr joint committee on nomenclature, Acta Crystallogr. A, 33, 681–684, https://doi.org/10.1107/S0567739477001703, 1977.

Barak, P. and Nater, E. A.: The Virtual Museum of Minerals and Molecules: molecular visualization in a virtual hands-on museum, J. Nat. Resour. Life Sci. Educ., 24, 67–71, 2005.

Brauner, K. and Preisinger, A.: Structur und entstehung des sepioliths, Tsh. Min. Pet. Mitt., 6, 120–140, https://doi.org/10.1007/BF01128033, 1956.

Brimhall, G. H., Agee, C., and Stoffregen, R.: The hydrothermal conversion of hornblende to biotite, Can. Mineral., 23, 369–379, 1985.

Brown, M. K., Hartling, D., Tailor, H. N., Van Wieren, K., Houghton, G. B., McGregor, I. G., Hansen, C. D., and Merbouh, N.: Piecewise 3D printing of crystallographic data for post-printing construction, CrystEngComm, 21, 5757–5766, https://doi.org/10.1039/C9CE00986H, 2019.

Cameron, M., Sueno, S., Prewitt, C. T., and Papike, J. J.: High-temperature crystal chemistry of acmite, diopside, hedenbergite, jadeite, spodumene, and ureyite, Am. Mineral., 58, 594–618, 1973.

Capitani, G. C. and Mellini, M.: The crystal structure of a second antigorite polysome ($m = 16$), by single-crystal synchrotron diffraction, Am. Mineral., 91, 394–399, https://doi.org/10.2138/am.2006.1919, 2006.

Carlson, W. D., Swinnea, J. S., and Miser, D. E.: Stability of orthoenstatite at high temperature and low pressure, Am. Mineral., 73, 1255–1263, 1988.

Deer, W. A., Howie, R. A., and Zussman, J.: An introduction to the rock-forming minerals, 3rd Edn., The Mineralogical Society, London, UK, https://doi.org/10.1180/DHZ, 2013.

Demichelis, R., De La Pierre, M., Mookherjee, M., Zicovich-Wilson, C. M., and Orlando, R.: Serpentine polymorphism: a quantitative insight from first-principles calculations, CrystEngComm, 18, 4412–4419, 2016.

Dixon, J. B.: Kaolin and Serpentine Group Minerals, in: Minerals in Soil Environments, 2nd Edn., edited by: Dixon, J. B. and Weed, S. B, SSSA Book Series, no. 1, 467–525, https://doi.org/10.2136/sssabookser1.2ed, 1989.

Dyar, M. D., Gunter, M. E., Davis, J. C., and Odell, M. R. L.: Integration of new methods into teaching mineralogy, J. Geosci. Educ., 52, 23–30, 2004.

Fahey, J. J., Ross, M., and Axelrod, J. M.: Loughlinite, a new hydrous sodium magnesium silicate, Am. Mineral., 45, 270–281, 1960.

Ferraris, G. and Gula, A.: Polysomatic aspects of microporous minerals – Heterophyllosilicates, palysepioles, and rhodesite-related structures, Rev. Min. Geochem., 57, 69–104, https://doi.org/10.2138/rmg.2005.57.3, 2005.

Ferraris, G., Khomyakov, A. P., Belluso, E., and Soboleva, S.V.: Kalifersite, a new alkaline silicate from Kola Peninsula (Russia) based on a palygorskite-sepiolite polysomatic series, Eur. J. Mineral., 10, 865–874, 1998.

Ferraris, G., Makovicky, E., and Merlino, S. (Eds.): Modularity at crystal scale – Twinning, in: Crystallography of Modular Materials, Oxford University Press, Oxford, UK, https://doi.org/10.1093/acprof:oso/9780199545698.003.0005, 2008.

Fischer, K. F.: A further refinement of the crystal structure of cummingtonite, $(Mg,Fe)_7(Si_4O_{11})_2(OH)_2$, Am. Mineral., 51, 814–818, 1966.

Guggenheim, S., Adams, J. M., Bain, D. C., Bergaya, F., Brigatti, M. F., Drits, V. A., Formoso, M. L. L., Galán, E., Kogure, T., and Stanjek, H.: Summary of recommendations of nomenclature committees relevant to clay mineralogy: Report of the association international pour l'etude des argiles (AIPEA) nomenclature committee for 2006, Clay. Clay Miner., 54, 761–772, 2006.

Hartman, P. and Perdok, W. G.: On the relations between structure and morphology of crystals. I, Acta. Crystallogr., 8, 49–52, https://doi.org/10.1107/S0365110X55000121, 1955.

Hawthorne, F. C., Oberti, R., Harlow, G. E., Maresch, W. V., Martin, R. F., Schumacher, J. C., and Welch, M. D.: Nomenclature of the amphibole supergroup, Am. Mineral., 97, 2031–2048, 2012.

Hendricks, S. B. and Jefferson, M. E.: Polymorphism of the micas with optical measurements, Am. Mineral., 24, 729–771, 1939.

Jahn, S. and Martonak, R.: Phase behavior of protoenstatite at high pressure studied by atomistic simulations, Am. Mineral., 94, 950–956, https://doi.org/10.2138/am.2009.3118, 2009.

Johannsen, A.: Petrographic terms for field use, J. Geol., 19, 317–332, 1911.

Jones, R., Haufe, P., Sells, E., Iravani, P., Olliver, V., Palmer, C., and Bowyer, A.: Reprap – The replicating rapid prototype, Robotica, 29, 177–191, 2011.

Kintel, M.: OpenSCAD, GitHub [code], https://github.com/openscad/openscad/, last access: 6 February 2021.

Leung, D. D. and McDonald, A. M.: Windmountainite, $\square Fe_2^{3+}Mg_2Si_8O_{20}(OH)_2(H_2O)_4 \cdot 4H_2O$, a new modulated, layered Fe^{3+}-Mg-silicate-hydrate from Wind Mountain, New Mexico: Characterisation and origin, with comments on the classification of palygorskite-group minerals, Can. Mineral., 58, 477–509, 2020.

Leung, D. D. V.: derekdvleung/totblocks: Totblocks 2022.05 (totblocks-2022.05), Zenodo [code], https://doi.org/10.5281/zenodo.5240816, 2022.

Liebau, F. (Ed.): Crystal chemical classification of silicate anions, in: Structural Chemistry of Silicates: Structure, Bonding and Classification, Springer-Verlag, Berlin, Germany, 52–68, https://doi.org/10.1007/978-3-642-50076-3, 1985.

McDonough, W. F. and Rudnick, R. L.: Mineralogy and composition of the upper mantle, Rev. Mineral. Geochem., 37, 139–164, 1998.

Mellini, M.: The crystal structure of lizardite 1*T*: Hydrogen bonds and polytypism, Am. Mineral., 67, 587–598, 1982.

Miramodus Ltd. Company: Miramodus alphabetic list of molecular models and crystal structure models: https://www.miramodus.com/molecular-models/beevers-models/alphabetic-index.shtml, last access: 3 December 2021.

Momma, K. and Izumi, F.: VESTA 3 for three-dimensional visualization of crystal, volumentric and morphology data, J. Appl. Crystallogr., 44, 1272–1276, 2011.

Moorefield-Lang, H. M.: Makers in the library: case studies of 3D printers and maker spaces in library settings, Libr. Hi Tech., 32, 583–593, https://doi.org/10.1108/LHT-06-2014-0056, 2014.

Morimoto, N., Fabries, J., Ferguson, A. K., Ginzburg, I. V., Ross, M., Seifert, F. A., Zussman, J., Aoki, K., and Gottardi, G.: Nomenclature of pyroxenes, Am. Mineral., 73, 1123–1133, 1988.

Nagai, T., Hattori, T., and Yamanaka, T., Compression mechanism of brucite: An investigation by structural refinement under pressure, Am. Mineral., 85, 760–764, https://doi.org/10.2138/am-2000-5-615, 2000.

Nespolo, M. and Bouznari, K.: Modularity of crystal structures: a unifying model for the biopyribole-palysepiole series, Eur. J. Mineral., 29, 369–383, https://doi.org/10.1127/ejm/2017/0029-2632, 2017.

Pasero, M.: The new IMA list of minerals – A work in progress, International Mineralogical Association, Commission on New Minerals, Nomenclature and Classification (IMA-CNMNC), http://cnmnc.main.jp/, last access: 1 February 2020.

Post, J. E., Bish, D. L., and Heaney, P. J.: Synchrotron powder X-ray diffraction study of the structure and dehydration behavior of sepiolite, Am. Mineral., 92, 91–97, https://doi.org/10.2138/am.2007.2134, 2007.

Pluth, J. J., Smith, J. V., Pushcharovsky, D. Y., Semenov, E. I., Bram, A., Riekel, C., Weber, H.-P., and Broach, R. W.: Third-generation synchrotron x-ray diffraction of 6-µm crystal of raite, $\approx Na_3Mn_3Ti_{0.25}Si_8O_{20}(OH)_2 \cdot 10H_2O$, P. Natl. Acad. Sci. USA, 94, 12263–12267, https://doi.org/10.1073/pnas.94.23.12263, 1997.

Prato, S. C. and Britton, L.: Digital fabrication technology in the library: Where we are and where we are going, J. Assoc. Inf. Sci. Tech., 42, 12–15, 2016.

Prusa, J.: Prusa3D, GitHub [code], https://github.com/prusa3d, last access: 16 July 2021.

Pryor, S.: Implementing a 3D printing service in an academic library, J. Libr. Adm., 54, 1–10, https://doi.org/10.1080/01930826.2014.893110, 2014.

Ralph, J.: Mindat, https://mindat.org, last access: 1 February 2020.

Rieder, M., Cavazzini, G., D'Yakonov, Y. S., Frank-Kamenetskii, V. A., Gottardi, G., Guggenheim, S., Koval, P. V., Müller, G., Neiva, A. M. R., Radoslovich, E. W., Robert, J.-L., Sassi, F. P., Takeda, H., Weiss, Z., and Wones, D. R.: Nomenclature of the micas, Can. Mineral., 36, 905–912, 1998.

Rodenbough, P. P., Vanti, W. B., and Chan, S.-W.: 3D-printing crystallographic unit cells for learning materials science and engineering, J. Chem. Educ., 92, 1960–1962, https://doi.org/10.1021/acs.jchemed.5b00597, 2015.

Ronov, A. B. and Yaroshevsky, A. A.: Chemical Composition of the Earth's Crust, in: The Earth's Crust and Upper mantle, edited by: Hart, P. J., American Geophysical Union, 37–57, https://doi.org/10.1029/GM013p0037, 1969.

Simon, H. A.: The architecture of complexity, P. Am. Philos. Soc., 106, 467–482, 1962.

Takéuchi, Y.: Tropochemical cell-twinning: A structure-building mechanism in crystalline solids, edited by: Sunagawa, I., Akimoto, S., Kushiro, I., and Morimoto, N., Terra Scientific Publishing Company, Tokyo, Japan, 1997.

Thompson, J. B.: Recent discussions of pyroxenes and amphiboles, Am. Mineral., 55, 292–316, 1970.

Thompson, J. B.: Biopyriboles and polysomatic series, Am. Mineral., 63, 239–249, 1978.

Thompson, J. B.: An introduction to the mineralogy and petrology of the biopyriboles, Rev. Mineral. Geochem., 9A, 141–188, 1981.

Thompson, R. M., Yang, H., and Downs, R. T.: Ideal wollastonite and the structural relationship between the pyroxenoids and pyroxenes, Am. Mineral., 101, 2544–2553, https://doi.org/10.2138/am-2016-5683, 2016.

Tsui, C.-Y. and Treagust, D. F.: Introduction to multiple representations: their importance in biology and biological education, in: Multiple Representation in Biological Education, edited by: Treagust, D. F. and Tsui, C.-Y., Springer, 3–18, 2013.

Veblen, D. R. and Burnham, C. W.: New biopyriboles from Chester, Vermont: I. Descriptive mineralogy, Am. Mineral., 63, 1000–1009, 1978a.

Veblen, D. R. and Burnham, C. W.: New biopyriboles from Chester, Vermont: II. The crystal chemistry of jimthompsonite, clinojimthompsonite, and chesterite, and the amphibole-mica reaction, Am. Mineral., 63, 1053–1073, 1978b.

Warr, L.: IMA–CNMNC approved symbols, Mineral. Mag., 85, 291–320, 2021.

Wood, P. A., Sarjeant, A. A., Bruno, I. J., Macrae, C. F., Maynard-Casely, H. E., and Towler, M.: The next dimension of structural science communication: simple 3D printing directly from a crystal structure, CrystEngComm, 19, 690–698, 2017.

Zanazzi, P. F., Montagnoli, M., Nazzareni, S., and Comodi, P.: Structural effects of pressure on monoclinic chlorite: A single-crystal study, Am. Mineral., 92, 655–661, https://doi.org/10.2138/am.2007.2341, 2007.

Zoltai, T.: Amphibole asbestos mineralogy, Rev. Mineral. Geochem., 9A, 237–278, 1981.